

# A New Correlator to Detect and Characterize the Chiral Magnetic Effect

Niseem Magdy,<sup>1,\*</sup> Shuzhe Shi,<sup>2</sup> Jinfeng Liao,<sup>2</sup> N. Ajitanand,<sup>1</sup> and Roy A. Lacey<sup>1,†</sup>

<sup>1</sup>*Department of Chemistry, State University of New York, Stony Brook, New York 11794, USA*

<sup>2</sup>*Physics Department and Center for Exploration of Energy and Matter,*

*Indiana University, 2401 N Milo B. Sampson Lane, Bloomington, IN 47408, USA.*

(Dated: October 11, 2021)

A charge-sensitive in-event correlator is proposed and tested for its efficacy to detect and characterize charge separation associated with the Chiral Magnetic Effect (CME) in heavy ion collisions. Tests, performed with the aid of two reaction models, indicate discernible responses for background- and CME-driven charge separation, relative to the second- ( $\Psi_2$ ) and third-order ( $\Psi_3$ ) event planes, which could serve to identify the CME. The tests also indicate a degree of sensitivity which would enable robust characterization of the CME via Anomalous Viscous Fluid Dynamics (AVFD) model comparisons.

PACS numbers: 25.75.-q, 25.75.Gz, 25.75.Ld

High-energy nuclear collisions at the Relativistic Heavy Ion Collider (RHIC) and the Large Hadron Collider (LHC) can result in the creation of a plasma composed of strongly coupled chiral quarks and gluons or the Quark-Gluon Plasma (QGP). Topological transitions such as sphalerons [1, 2], which occur frequently in the QGP [3, 4], can induce a net axial charge asymmetry of the chiral quarks which fluctuate from event to event. In the presence of the strong electromagnetic  $\vec{B}$ -fields created in the same collisions, this chiral anomaly is predicted to convert into an electric current which produces a final-state charge separation known as the Chiral Magnetic Effect (CME) [5–10]. For recent reviews, see e.g. [11–13].

The electric current  $\vec{J}_Q$ , created along the  $\vec{B}$ -field, stems from anomalous chiral transport of the chiral fermions in the QGP:

$$\vec{J}_Q = \sigma_5 \vec{B}, \quad \sigma_5 = \mu_5 \frac{Q^2}{4\pi^2}, \quad (1)$$

where  $\sigma_5$  is the chiral magnetic conductivity,  $\mu_5$  is the chiral chemical potential that quantifies the axial charge asymmetry or imbalance between right-handed and left-handed quarks in the plasma, and  $Q$  is the quark electric charge [8, 14–16]. Thus, experimental observation of its associated charge separation, could provide crucial insights on anomalous transport and the interplay of chiral symmetry restoration, axial anomaly, and gluonic topology in the QGP.

The  $\vec{B}$ -field, which is strongly time-dependent [17–19], is generated perpendicular to the reaction plane ( $\Psi_{\text{RP}}$ ) defined by the impact parameter and the beam axis. Consequently, CME-driven charge separation can be identified and characterized via the first  $P$ -odd sine term ( $a_1$ ) in a Fourier decomposition of the charged-particle azimuthal distribution [20]:

$$\frac{dN^{\text{ch}}}{d\phi} \propto [1 + 2 \sum_n v_n \cos(n\Delta\phi) + a_n \sin(n\Delta\phi) + \dots] \quad (2)$$

where  $\Delta\phi = \phi - \Psi_{\text{RP}}$  gives the particle azimuthal angle with respect to the reaction plane angle, and  $v_n$  and  $a_n$  denote the coefficients of  $P$ -even and  $P$ -odd Fourier terms, respectively. The second-order event plane,  $\Psi_2$ , determined by the maximal particle density in the elliptic azimuthal anisotropy and the beam axis, is usually employed as a proxy for  $\Psi_{\text{RP}}$  in experimental measurements. Here, it is noteworthy that the third-order event plane,  $\Psi_3$ , can not be used to detect CME-driven charge separation, since there is little, if any, correlation between  $\Psi_{\text{RP}}$  and  $\Psi_3$ . The event-by-event fluctuations contribute to an event-wise de-correlation between the magnetic field direction imposed by  $\Psi_{\text{RP}}$ , and the orientation of  $\Psi_2$  imposed by the bulk collision geometry [21]. The dispersion of  $\Psi_2$  about  $\Psi_{\text{RP}}$  reduces the magnitude of  $a_1$ , which depends on both the initial axial charge and the time evolution of the magnetic field (c.f. Eq. 1). The latter are both not well constrained theoretically.

The charge-dependent correlator,  $\gamma_{\alpha\beta}$ , has been widely used at RHIC [22–28] and the LHC [29, 30] in ongoing attempts to identify and quantify CME-driven charge separation:

$$\gamma_{\alpha\beta} = \left\langle \cos(\phi_\alpha^{(\pm)} + \phi_\beta^{(\pm)} - 2\Psi_2) \right\rangle, \quad (3)$$

where  $\phi_\alpha, \phi_\beta$  denote the azimuthal emission angles for like-sign ( $++$  or  $--$ ) and unlike-sign ( $+-$ ) particle pairs. A charge-dependent azimuthal correlation, qualitatively consistent with the expectation for CME-driven charge separation, has been observed in these measurements. However, they remain inconclusive because of several identified sources of background correlations that can account for most, if not all, of the measurements [31–35]. A recent cause for pause, is the observation that the charge-dependent azimuthal correlations for p+Pb and Pb+Pb collisions, have nearly identical values for similar multiplicity selections [30]. This poses a significant challenge for the use of the  $\gamma_{\alpha\beta}$  correlator in such measurements, because CME-induced charge separation is predicted to be negligible in p+Pb collisions. That is,

the absence of a strong correlation between the orientation of the  $\Psi_2$  plane and the  $\vec{B}$ -field in p+Pb collisions, should result in very little, if any, CME-driven charge separation [30, 36, 37].

To a large extent, the present ambiguity between background- and CME-driven charge separation, stems from the fact that the  $\gamma_{\alpha\beta}$  correlator gives the same qualitative response to both. Thus, new measurements and improved data analysis methodologies, designed to suppress or separate background contributions from genuine CME-driven charge separation, are required for robust identification and characterization of the CME [? ].

In this work we present and validate the response of a new charge-sensitive correlator, specifically designed to give distinct discernible responses for background- and CME-driven charge separation relative to the  $\Psi_2$  and  $\Psi_3$  event planes. The tests are performed with A Multi-Phase Transport Model (AMPT) [38] and the Anomalous Viscous Fluid Dynamics (AVFD) model [10]. Both models are known to give a good representation of the experimentally measured particle yields, spectra, flow, etc. Therefore, they both can provide a good estimate of the magnitude and nature of the purely background-driven charge separation signal expected in the data samples collected at RHIC and the LHC.

Anomalous transport from the CME, is also implemented in the AVFD model [10]. This important feature, facilitates our study of the correlators' response to the combined influence of the backgrounds and an input CME-driven charge separation signal. The model uses Monte Carlo Glauber initial conditions to simulate the evolution of fermion currents in the QGP, on top of the bulk fluid evolution implemented in the VISHNU hydrodynamic code, followed by a URQMD hadron cascade stage. A time-dependent magnetic field  $B(\tau) = \frac{B_0}{1+(\tau/\tau_B)^2}$ , acting in concert with a nonzero initial axial charge density, is used to generate a CME current (embedded in the fluid dynamical equations) leading to a charge separation along the magnetic field. The peak values  $B_0$ , obtained from event-by-event simulations [21], are used with a relatively conservative lifetime  $\tau_B = 0.6$  fm/c. For the initial axial charge density arising from gluonic topological charge fluctuations, we adopt the commonly used estimate based on the strong chromo-electromagnetic fields in the early-stage glasma. A More in-depth account of the implementation of the AVFD model can be found in Refs. [10] and [? ].

The new correlators  $R_{\Psi_m}(\Delta S)$ , are constructed for each event plane  $\Psi_m$ , as the ratio:

$$R_{\Psi_m}(\Delta S) = C_{\Psi_m}(\Delta S)/C_{\Psi_m}^{\perp}(\Delta S), \quad m = 2, 3, \quad (4)$$

where  $C_{\Psi_m}(\Delta S)$  and  $C_{\Psi_m}^{\perp}(\Delta S)$  are correlation functions designed to quantify charge separation  $\Delta S$ , parallel and perpendicular (respectively) to the  $\vec{B}$ -field, i.e., perpendicular and parallel (respectively) to  $\Psi_{\text{RP}}$ . Since CME-driven charge separation occurs only along the  $\vec{B}$ -field

and  $\Psi_2$  and  $\Psi_{\text{RP}}$  are strongly correlated,  $C_{\Psi_2}(\Delta S)$  measures both CME- and background-driven charge separation. In contrast,  $C_{\Psi_2}^{\perp}(\Delta S)$  measures only background-driven charge separation. The absence of a strong correlation between the orientation of the  $\Psi_3$  plane and the  $\vec{B}$ -field, also renders  $C_{\Psi_3}(\Delta S)$  and  $C_{\Psi_3}^{\perp}(\Delta S)$  insensitive to a CME-driven charge separation. However, they provide crucial insight on the relative importance of background-driven charge separation as discussed below.

The correlation functions used to quantify charge separation parallel to the  $\vec{B}$ -field, are constructed from the ratio of two distributions [39]:

$$C_{\Psi_m}(\Delta S) = \frac{N_{\text{real}}(\Delta S)}{N_{\text{Shuffled}}(\Delta S)}, \quad m = 2, 3, \quad (5)$$

where  $N_{\text{real}}(\Delta S)$  is the distribution over events, of charge separation relative to the  $\Psi_m$  planes in each event:

$$\Delta S = \frac{\sum_1^p \sin(\frac{m}{2} \Delta\varphi_m)}{p} - \frac{\sum_n^n \sin(\frac{m}{2} \Delta\varphi_m)}{n}, \quad (6)$$

where  $n$  and  $p$  are the numbers of negatively- and positively charged hadrons in an event,  $\Delta\varphi_m = \phi - \Psi_m$  and  $\phi$  is the azimuthal emission angle of the charged hadrons. The  $N_{\text{Shuffled}}(\Delta S)$  distribution is similarly obtained from the same events, following random reassignment (shuffling) of the charge of each particle in an event. This procedure ensures identical properties for the numerator and the denominator in Eq. 5, except for the charge-dependent correlations which are of interest.

The correlation functions  $C_{\Psi_m}^{\perp}(\Delta S)$ , used to quantify charge separation perpendicular to the  $\vec{B}$ -field, are constructed with the same procedure outlined for  $C_{\Psi_m}(\Delta S)$ , but with  $\Psi_m$  replaced by  $\Psi_m + \pi/m$ . This  $\pi/m$  rotation of the event plane, guarantees that a possible CME-driven charge separation does not contribute to these correlation functions.

The correlator  $R_{\Psi_2}(\Delta S) = C_{\Psi_2}(\Delta S)/C_{\Psi_2}^{\perp}(\Delta S)$ , gives a measure of the magnitude of charge separation parallel to the  $\vec{B}$ -field (perpendicular to  $\Psi_2$ ), relative to that for charge separation perpendicular to the  $\vec{B}$ -field (parallel to  $\Psi_2$ ). Since the CME occurs along the  $\vec{B}$ -field, correlations dominated by CME-driven charge separation should result in concave-shaped distributions having widths that reflect the magnitude  $a_1$  of the charge separation (cf. Eq. 2). That is, the stronger the CME-driven charge separation, the narrower the  $R_{\Psi_2}(\Delta S)$  distribution. In contrast, the correlator  $R_{\Psi_3}(\Delta S) = C_{\Psi_3}(\Delta S)/C_{\Psi_3}^{\perp}(\Delta S)$  would be insensitive to this CME-driven charge separation, due to the absence of a strong correlation between the orientation of the  $\Psi_3$  plane and the  $\vec{B}$ -field.

For background-driven charge separation, similar patterns are to be expected for both the  $R_{\Psi_2}(\Delta S)$  and

$R_{\Psi_3}(\Delta S)$  distributions. Note as well, that such patterns could be convex- or concave-shaped [? ], depending on the detailed nature of the background-driven correlations. Therefore, in addition to an observed concave-shaped distribution for  $R_{\Psi_2}(\Delta S)$ , an observed difference between the distributions for  $R_{\Psi_2}(\Delta S)$  and  $R_{\Psi_3}(\Delta S)$  is essential for CME identification and characterization.

The magnitude of a CME-driven charge separation is reflected in the width of the concave-shaped distribution for  $R_{\Psi_2}(\Delta S)$ , which is also influenced by particle number fluctuations and the resolution of  $\Psi_2$ . That is, stronger CME-driven signals lead to narrower concave-shaped distributions (smaller widths), which are made broader by particle number fluctuations and poorer event-plane resolutions. The influence of the particle number fluctuations can be minimized by scaling  $\Delta S$  by the width  $\sigma_{\Delta S_{\text{sh}}}$  of the distribution for  $N_{\text{shuffled}}(\Delta S)$  *i.e.*,  $\Delta S' = \Delta S / \sigma_{\Delta S_{\text{sh}}}$ . Similarly, the effects of the event plane resolution can be accounted for by scaling  $\Delta S'$  by the resolution factor  $\delta_{\text{Res}}$ , *i.e.*,  $\Delta S'' = \Delta S' / \delta_{\text{Res}}$ , where  $\delta_{\text{Res}}$  is the event plane resolution. The efficacy of these scaling factors have been confirmed via detailed simulation studies, as well as with actual data.

Simulated events from both the AMPT and AVFD models were used to study the response, as well as the efficacy of the  $R_{\Psi_m}(\Delta S)$  correlators. Representative results from these studies are summarized in Figs. 1 - 5.

The response of the correlator to background- and CME-driven charge separation is illustrated in Fig. 1. Panel (a) indicates that the  $R_{\Psi_2}(\Delta S)$  correlator exhibits a convex-shaped distribution for the background-driven ( $a_1 = 0$ ) charge separation in both models, albeit with some model dependence for the magnitudes. Note that these background-driven distributions are not required to be convex-shaped [? ] and are specific to these models. Panel (b) shows that the introduction of a modest input CME-driven charge separation ( $a_1 = 1.0\%$ ) in the same AVFD events, results in a change from convex-shaped to a concave-shaped distribution for  $R_{\Psi_2}(\Delta S)$ . This change reflects the influence of the CME-driven charge separation in the AVFD model. These patterns contrast with those of the  $\gamma_{\alpha\beta}$  correlator, which was observed to give the same qualitative response to both background-driven and CME-driven charge separation in AMPT model simulations [? ].

Figure 2 show background-driven charge separation distributions for both  $R_{\Psi_2}(\Delta S)$  and  $R_{\Psi_3}(\Delta S)$ , obtained with the AMPT model. Panels (a) and (b) show distributions which are corrected for number fluctuations ( $\Delta S'$ ) and the combined effects of number fluctuations and event plane resolution ( $\Delta S''$ ) respectively. Fig. 2(b) indicate the expected similarity between the shape and widths for  $R_{\Psi_2}(\Delta S'')$  and  $R_{\Psi_3}(\Delta S'')$ . This similarity is especially important since  $R_{\Psi_3}(\Delta S)$  is insensitive to CME-driven charge separation. Thus, a discernible difference in the response for  $R_{\Psi_2}(\Delta S'')$  and  $R_{\Psi_3}(\Delta S'')$

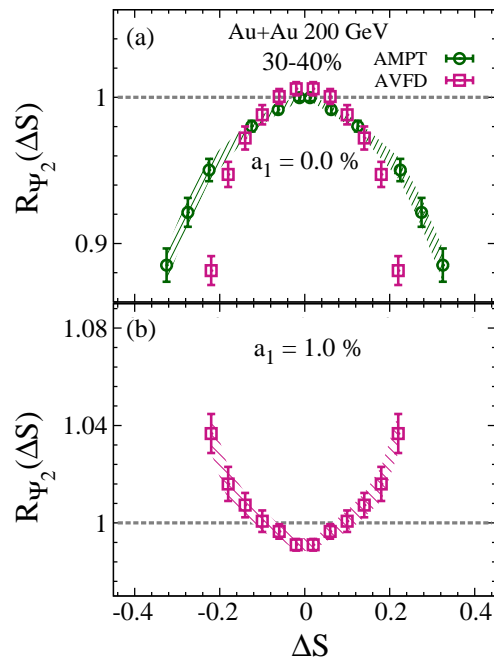


FIG. 1. Comparison of the  $R(\Delta S)$  correlators for (a) background-driven charge separation ( $a_1 = 0$ ) in 30-40% Au+Au collisions ( $\sqrt{s_{\text{NN}}} = 200$  GeV) obtained with the AMPT and AVFD models, and (b) the combined effects of background- and CME-driven ( $a_1 = 1.0\%$ ) charge separation in Au+Au collisions obtained with the AVFD model at the same centrality and beam energy.

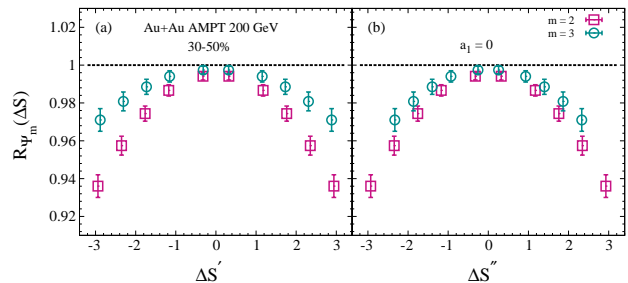


FIG. 2. Comparison of the  $R_{\Psi_m}(\Delta S')$  (a) and  $R_{\Psi_m}(\Delta S'')$  (b) correlators for background-driven charge separation ( $a_1 = 0$ ) in 30-50% Au+Au collisions ( $\sqrt{s_{\text{NN}}} = 200$  GeV) obtained with the AMPT model.

constitutes a crucial and necessary requirement for unambiguous identification and characterization of CME-driven charge separation. In the same vein,  $R_{\Psi_2}(\Delta S)$  would not be expected to show a significant concave-shaped response in p(d)+A collisions, due to the absence of a strong correlation between the orientation of the  $\Psi_2$  plane and the  $\vec{B}$ -field in these collisions [30, 36, 37].

The sensitivity of the  $R_{\Psi_2}(\Delta S)$  correlator to varying degrees of input CME-driven charge separation (characterized by  $a_1$ ) at a fixed collision centrality, is shown in Fig. 3. Note that for a fixed centrality, a change in the

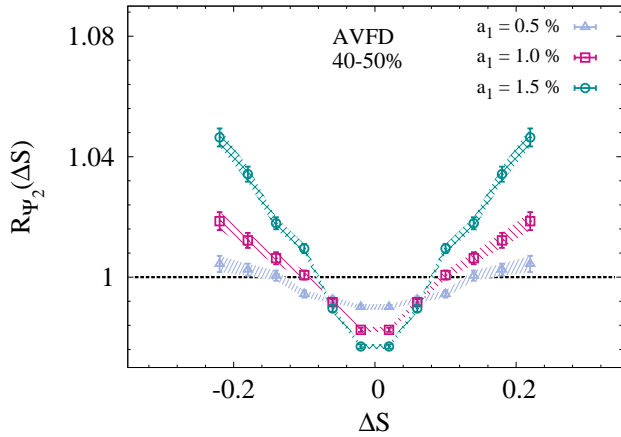


FIG. 3. Comparison of the  $R_{\Psi_2}(\Delta S)$  correlator for different input charge separation signals characterized by  $a_1$ , in 40-50% central Au+Au ( $\sqrt{s_{\text{NN}}} = 200$  GeV) events obtained with AVFD model.

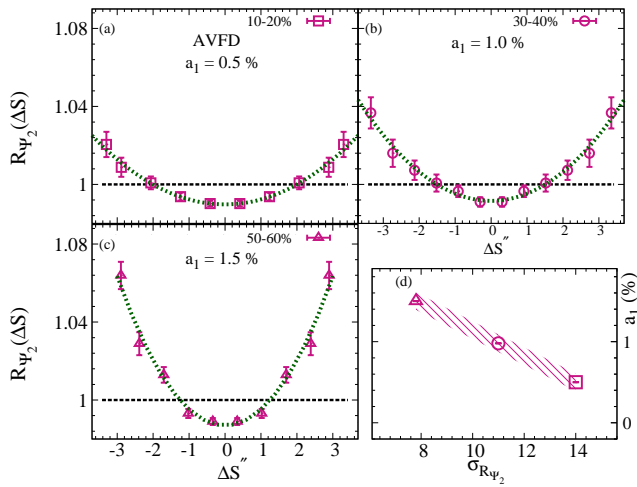


FIG. 4. Comparison of the  $R_{\Psi_2}(\Delta S'')$  correlator obtained from the analysis of (a) 10-20%, (b) 30-40% and (c) 50-60% central AVFD events for Au+Au collisions at  $\sqrt{s_{\text{NN}}} = 200$  GeV. The curves represent Gaussian fits to the distributions; (d)  $a_1$  vs.  $\sigma_{R_{\Psi_2}}$  for the fits indicated indicated in (a), (b) and (c).

value of  $a_1$  is tantamount to a change in the input value of the initial chiral anomaly in AVFD. Note as well that, for a fixed centrality, the event plane resolution is the same for events generated with different values of  $a_1$ . A concave-shaped distribution can be observed in each case, confirming the presence of the input CME-driven signals. The amplitudes of these distributions also track with the magnitude of  $a_1$ , indicating that the  $R_{\Psi_2}(\Delta S)$  correlator is not only suited for CME-driven signal identification, but also for signal characterization.

The sensitivity of the  $R_{\Psi_2}(\Delta S)$  correlator to the influence of the  $\vec{B}$ -field in AVFD, can also be studied via the centrality dependence of  $R_{\Psi_2}(\Delta S)$ . Figs. 4(a), (b) and (c) show the correlator distributions for 10 – 20%,

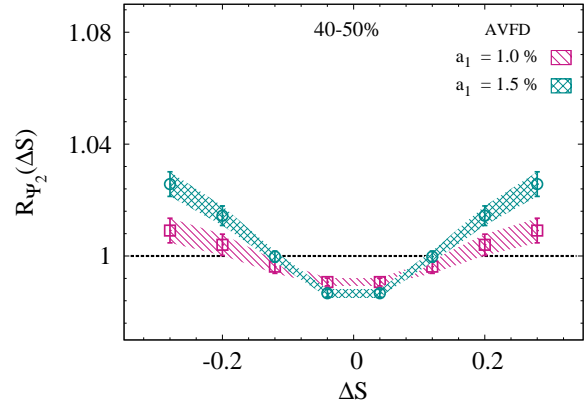


FIG. 5. Comparison of the  $R_{\Psi_2}(\Delta S)$  correlators obtained from AVFD events with  $a_1 = 1\%$  and  $1.5\%$ . The AVFD results are generated with an event plane resolution and  $p_T$  and  $\eta$  cuts, similar to the experimental ones [37].

30 – 40% and 50 – 60% central Au+Au collisions respectively. For these plots, we have scaled  $\Delta S$  to account for the difference in the associated number fluctuations and event plane resolution ( $\Delta S''$ ). The concave-shaped distribution, apparent in each panel, confirms the input CME-driven signal in each case. The widths of these distributions  $\sigma_{R_{\Psi_2}}$ , also reflect the increase of  $a_1$  as collisions become more peripheral (panel (d)). This confirms the trend expected for the magnitude of the  $\vec{B}$ -field with collision centrality. The implied sensitivity of  $R_{\Psi_2}(\Delta S)$  to the  $\vec{B}$ -field, could also provide an independent approach to the detection and quantification of the CME in isobaric collision.

For model comparisons to actual experimental data, it is also necessary to impose the experimental cuts ( $|\eta| \sim 0.8$  and  $p_T \geq 0.35$  GeV/c [37]), as well as account for any difference between the experimental and simulated event plane resolution. Fig. 5 compares the results from AVFD for two values of  $a_1$ , when the experimental cuts and the event plane resolution are taken into account. These  $R(\Delta S)$  distributions are still concave-shaped, albeit with smaller amplitudes than the corresponding distributions shown in Fig. 3, due to the effects of the kinematic cuts and the event plane resolution. A rudimentary comparison of these distributions to preliminary STAR Au+Au data for the same centrality and beam energy [37] shows good agreement between the data and AVFD results for  $a_1 = 1\%$ , suggesting the presence of a small CME-driven charge separation in 40-50% central Au+Au collisions at  $\sqrt{s_{\text{NN}}} = 200$  GeV.

In summary, we have presented new  $R_{\Psi_m}(\Delta S)$  correlators which are well suited for studying the CME. Validation tests, performed with the AMPT and AVFD models, indicate that the correlator gives discernible responses for background- and CME-driven charge separation, which could allow unambiguous identification of the CME via  $R_{\Psi_2}(\Delta S)$  and  $R_{\Psi_3}(\Delta S)$  measurements. The tests also in-

dicating a degree of sensitivity which would enable a robust characterization of experimental CME-driven charge separation signals with magnitudes comparable to those currently simulated in the AVFD model. An initial comparison of the correlators obtained from preliminary data and AVFD calculations, suggests the presence of a CME-driven charge separation in 40-50% central Au+Au collisions at  $\sqrt{s_{NN}} = 200$  GeV. A vigorous effort is currently underway to extract the experimental and theoretical differential  $R_{\Psi_m}(\Delta S)$  correlators for different systems and energies, to characterize the CME in RHIC and LHC collisions. The  $R_{\Psi_m}(\Delta S)$  correlators also provide an independent approach to the detection and quantification of the CME in the upcoming isobaric collision experiments at RHIC.

### ACKNOWLEDGMENTS

This research is supported by the US Department of Energy, Office of Science, Office of Nuclear Physics, under contract DE-FG02-87ER40331.A008 (NM, NA and RL) and by the National Science Foundation under Grant No. PHY-1352368 (SS and JL). The AVFD study is based upon work supported by the U.S. Department of Energy, Office of Science, Office of Nuclear Physics, within the framework of the Beam Energy Scan Theory (BEST) Topical Collaboration.

---

\* niseemm@gmail.com

† Roy.Lacey@stonybrook.edu

- [1] Frans R. Klinkhamer and N. S. Manton, "A Saddle Point Solution in the Weinberg-Salam Theory," *Phys. Rev.* **D30**, 2212 (1984).
- [2] Peter Brockway Arnold and Larry D. McLerran, "Sphalerons, Small Fluctuations and Baryon Number Violation in Electroweak Theory," *Phys. Rev.* **D36**, 581 (1987).
- [3] Guy D. Moore and Marcus Tassler, "The Sphaleron Rate in SU(N) Gauge Theory," *JHEP* **02**, 105 (2011), [arXiv:1011.1167 \[hep-ph\]](#).
- [4] M. Mace, S. Schlichting, and R. Venugopalan, "Off-equilibrium sphaleron transitions in the Glasma," *Phys. Rev.* **D93**, 074036 (2016), [arXiv:1601.07342 \[hep-ph\]](#).
- [5] Dmitri Kharzeev, "Parity violation in hot QCD: Why it can happen, and how to look for it," *Phys. Lett.* **B633**, 260–264 (2006), [arXiv:hep-ph/0406125](#).
- [6] D. Kharzeev and A. Zhitnitsky, "Charge separation induced by P-odd bubbles in QCD matter," *Nucl. Phys.* **A797**, 67–79 (2007), [arXiv:0706.1026 \[hep-ph\]](#).
- [7] Dmitri E. Kharzeev, Larry D. McLerran, and Harmen J. Warringa, "The Effects of topological charge change in heavy ion collisions: 'Event by event P and CP violation'," *Nucl. Phys.* **A803**, 227–253 (2008), [arXiv:0711.0950 \[hep-ph\]](#).
- [8] Kenji Fukushima, Dmitri E. Kharzeev, and Harmen J. Warringa, "The Chiral Magnetic Effect," *Phys. Rev.* **D78**, 074033 (2008), [arXiv:0808.3382 \[hep-ph\]](#).
- [9] Dmitri E. Kharzeev and Dam T. Son, "Testing the chiral magnetic and chiral vortical effects in heavy ion collisions," *Phys. Rev. Lett.* **106**, 062301 (2011), [arXiv:1010.0038 \[hep-ph\]](#).
- [10] Yin Jiang, Shuzhe Shi, Yi Yin, and Jinfeng Liao, "Quantifying Chiral Magnetic Effect from Anomalous-Viscous Fluid Dynamics," (2016), [arXiv:1611.04586 \[nucl-th\]](#).
- [11] Dmitri E. Kharzeev, "The Chiral Magnetic Effect and Anomaly-Induced Transport," *Prog. Part. Nucl. Phys.* **75**, 133–151 (2014), [arXiv:1312.3348 \[hep-ph\]](#).
- [12] Jinfeng Liao, "Anomalous transport effects and possible environmental symmetry violation in heavy-ion collisions," *Pramana* **84**, 901–926 (2015), [arXiv:1401.2500 \[hep-ph\]](#).
- [13] D. E. Kharzeev, J. Liao, S. A. Voloshin, and G. Wang, "Chiral magnetic and vortical effects in high-energy nuclear collisions: A status report," *Prog. Part. Nucl. Phys.* **88**, 1–28 (2016), [arXiv:1511.04050 \[hep-ph\]](#).
- [14] Dam T. Son and Piotr Surowka, "Hydrodynamics with Triangle Anomalies," *Phys. Rev. Lett.* **103**, 191601 (2009), [arXiv:0906.5044 \[hep-th\]](#).
- [15] Valentin I. Zakharov, "Chiral Magnetic Effect in Hydrodynamic Approximation," (2012), [10.1007/978-3-642-37305-3-11](#), [Lect. Notes Phys. 871,295(2013)], [arXiv:1210.2186 \[hep-ph\]](#).
- [16] Kenji Fukushima, "Views of the Chiral Magnetic Effect," *Lect. Notes Phys.* **871**, 241–259 (2013), [arXiv:1209.5064 \[hep-ph\]](#).
- [17] V. Skokov, A. Yu. Illarionov, and V. Toneev, "Estimate of the magnetic field strength in heavy-ion collisions," *Int. J. Mod. Phys.* **A24**, 5925–5932 (2009), [arXiv:0907.1396 \[nucl-th\]](#).
- [18] L. McLerran and V. Skokov, "Comments About the Electromagnetic Field in Heavy-Ion Collisions," *Nucl. Phys.* **A929**, 184–190 (2014), [arXiv:1305.0774 \[hep-ph\]](#).
- [19] Kirill Tuchin, "Electromagnetic field and the chiral magnetic effect in the quark-gluon plasma," *Phys. Rev.* **C91**, 064902 (2015), [arXiv:1411.1363 \[hep-ph\]](#).
- [20] Sergei A. Voloshin, "Parity violation in hot QCD: How to detect it," *Phys. Rev.* **C70**, 057901 (2004), [arXiv:hep-ph/0406311 \[hep-ph\]](#).
- [21] John Błoczynski, Xu-Guang Huang, Xilin Zhang, and Jinfeng Liao, "Azimuthally fluctuating magnetic field and its impacts on observables in heavy-ion collisions," *Phys. Lett.* **B718**, 1529–1535 (2013), [arXiv:1209.6594 \[nucl-th\]](#).
- [22] B. I. Abelev *et al.* (STAR), "Azimuthal Charged-Particle Correlations and Possible Local Strong Parity Violation," *Phys. Rev. Lett.* **103**, 251601 (2009), [arXiv:0909.1739 \[nucl-ex\]](#).
- [23] B. I. Abelev *et al.* (STAR), "Observation of charge-dependent azimuthal correlations and possible local strong parity violation in heavy

- ion collisions,” *Phys. Rev.* **C81**, 054908 (2010), [arXiv:0909.1717 \[nucl-ex\]](#).
- [24] L. Adamczyk *et al.* (STAR), “Fluctuations of charge separation perpendicular to the event plane and local parity violation in  $\sqrt{s_{NN}} = 200$  GeV Au+Au collisions at the BNL Relativistic Heavy Ion Collider,” *Phys. Rev.* **C88**, 064911 (2013), [arXiv:1302.3802 \[nucl-ex\]](#).
- [25] L. Adamczyk *et al.* (STAR), “Measurement of charge multiplicity asymmetry correlations in high-energy nucleus-nucleus collisions at  $\sqrt{s_{NN}} = 200$  GeV,” *Phys. Rev.* **C89**, 044908 (2014), [arXiv:1303.0901 \[nucl-ex\]](#).
- [26] L. Adamczyk *et al.* (STAR), “Beam-energy dependence of charge separation along the magnetic field in Au+Au collisions at RHIC,” *Phys. Rev. Lett.* **113**, 052302 (2014), [arXiv:1404.1433 \[nucl-ex\]](#).
- [27] Prithwish Tribedy (STAR), “Disentangling flow and signals of Chiral Magnetic Effect in U+U, Au+Au and p+Au collisions,” in *Quark Matter 2017, Chicago, Illinois, USA, 2017* (2017) [arXiv:1704.03845 \[nucl-ex\]](#).
- [28] Jie Zhao, Hanlin Li, and Fuqiang Wang, “Isolating backgrounds from the chiral magnetic effect,” (2017), [arXiv:1705.05410 \[nucl-ex\]](#).
- [29] Betty Abelev *et al.* (ALICE), “Charge separation relative to the reaction plane in Pb-Pb collisions at  $\sqrt{s_{NN}} = 2.76$  TeV,” *Phys. Rev. Lett.* **110**, 012301 (2013), [arXiv:1207.0900 \[nucl-ex\]](#).
- [30] Vardan Khachatryan *et al.* (CMS), “Observation of charge-dependent azimuthal correlations in pPb collisions and its implication for the search for the chiral magnetic effect,” Submitted to: *Phys. Rev. Lett* (2016), [arXiv:1610.00263 \[nucl-ex\]](#).
- [31] Fuqiang Wang, “Effects of Cluster Particle Correlations on Local Parity Violation Observables,” *Phys. Rev.* **C81**, 064902 (2010), [arXiv:0911.1482 \[nucl-ex\]](#).
- [32] Adam Bzdak, Volker Koch, and Jinfeng Liao, “Azimuthal correlations from transverse momentum conservation and possible local parity violation,” (2010), [arXiv:1008.4919 \[nucl-th\]](#).
- [33] Soren Schlichting and Scott Pratt, “Charge conservation at energies available at the BNL Relativistic Heavy Ion Collider and contributions to local parity violation observables,” *Phys. Rev.* **C83**, 014913 (2011), [arXiv:1009.4283 \[nucl-th\]](#).
- [34] Berndt Muller and Andreas Schafer, “Charge Fluctuations from the Chiral Magnetic Effect in Nuclear Collisions,” (2010), [arXiv:1009.1053 \[hep-ph\]](#).
- [35] Jinfeng Liao, Volker Koch, and Adam Bzdak, “On the Charge Separation Effect in Relativistic Heavy Ion Collisions,” *Phys. Rev.* **C82**, 054902 (2010), [arXiv:1005.5380 \[nucl-th\]](#).
- [36] R. Belmont and J. L. Nagle, “To CME or not to CME? Implications of p+Pb measurements of the chiral magnetic effect in heavy ion collisions,” *Phys. Rev.* **C96**, 024901 (2017), [arXiv:1610.07964 \[nucl-th\]](#).
- [37] Roy A. Lacey (For the STAR Collaboration), “Charge separation measurements in p(d)+A and A(B)+A collisions: Implications for characterization of the chiral magnetic effect,” Fudan University, Shanghai China, 2017, <https://indico.cern.ch/event/614524/contributions/2702626/a>
- [38] Zi-Wei Lin, Che Ming Ko, Bao-An Li, Bin Zhang, and Subrata Pal, “A Multi-phase transport model for relativistic heavy ion collisions,” *Phys. Rev.* **C72**, 064901 (2005), [arXiv:nucl-th/0411110 \[nucl-th\]](#).
- [39] N. N. Ajitanand, Roy A. Lacey, A. Taranenko, and J. M. Alexander, “A New method for the experimental study of topological effects in the quark-gluon plasma,” *Phys. Rev.* **C83**, 011901 (2011), [arXiv:1009.5624 \[nucl-ex\]](#).